

# APPLICATION OF STOCHASTIC MODELING TO ANALYSIS OF PHOTOMETRIC REVERBERATION MAPPING DATA

YING ZU<sup>1,2,3</sup>, C.S. KOCHANEK<sup>1,2</sup>, SZYMON KOZŁOWSKI<sup>4</sup>, AND B.M. PETERSON<sup>1,2</sup>

*Draft version September 25, 2018*

## ABSTRACT

We use both simulated and real quasar light curves to explore modeling photometric reverberation-mapping (RM) data as a stochastic process. We do this using modifications to our previously developed RM method based on modeling quasar variability as a damped random walk. We consider the feasibility of one and two-band photometric RM and compare the results with those from spectroscopic RM. We find that our method for two-band photometric RM can be competitive with spectroscopic RM only for strong (large equivalent width) lines like H $\alpha$  and H $\beta$ , and that the one-band method is also feasible, but requires very high-precision photometry. We fail to robustly detect H $\alpha$  lags in single-band quasar light curves from OGLE-III and IV despite the outstanding cadence and time span of the data, on account of photometric uncertainties in the range 0.02–0.04 mag. Simulations suggest that success could be achieved if the photometric uncertainties were of order 0.01 mag. Single-band RM for all lines and two-band RM for lower equivalent width lines are likely only feasible for statistical estimates of mean lags for large samples of AGN of similar properties (e.g., luminosity) rather than for individual quasars. Our approach is directly applicable to the time-domain programs within ongoing and future wide-field imaging surveys, and could provide robust lag measurements for an unprecedented number of systems.

*Keywords:* galaxies: active — galaxies: statistics — methods: data analysis — methods: numerical — methods: statistical

## 1. INTRODUCTION

Determination of the masses of the supermassive black holes (SMBHs) over cosmic history is of interest for a number of reasons. Unfortunately, most methods of measuring SMBH masses rely on high angular resolution and are thus currently feasible only in the local universe. It is possible, however, to measure the masses of the SMBHs at the centers of active galactic nuclei (AGNs), or quasars, by use of reverberation mapping (RM; Blandford & McKee 1982; Peterson 1993, 2014), which substitutes time resolution for angular resolution. While AGNs constitute only a trace population, they seem to show, for example, the same  $M_{\text{SMBH}}-\sigma_*$  relation (Ferrarese & Merritt 2000; Gebhardt et al. 2000; Ferrarese et al. 2001; Nelson et al. 2004; Onken et al. 2004; Dasyra et al. 2007; Woo et al. 2010; Graham et al. 2011; Park et al. 2012; Grier et al. 2013a) that has been driving studies of galaxy–SMBH co-evolution (Silk & Rees 1998; Fabian 1999; King 2003, 2005; Treu et al. 2004; Murray et al. 2005; Di Matteo et al. 2005, 2008; Peng et al. 2006; Shankar et al. 2009; Shankar 2009; Merloni et al. 2010). Moreover, the highest redshift quasars (e.g., Mortlock et al. 2011; De Rosa et al. 2014; Carnall et al. 2015; Jiang et al. 2015) put strong constraints on the SMBH formation and growth in the early universe

(e.g., Volonteri 2010; Latif et al. 2013; Latif & Volonteri 2015).

At the present time, published RM studies have for the most part been restricted to local AGNs (e.g., Peterson et al. 2004; Denney et al. 2010; Grier et al. 2012a; Bentz et al. 2013; Barth et al. 2015; De Rosa et al. 2015). Standard RM relies on the spectroscopic monitoring of broad-line fluxes, which are then cross-correlated with a continuum light curve, either also measured from the spectra, measured independently photometrically, or constructed from some combination of the two, to obtain the “lag” or time delay between continuum flux variations and the emission-line response. The lag is taken to be the light travel time from the central engine to the broad-line region (BLR). By combining the lag with a suitable measurement of the emission-line width  $\Delta V$ , which is taken to be an estimate of the virial motion of the BLR gas, one obtains an estimate for the mass of the SMBH

$$M_{\text{SMBH}} = f \frac{c\tau\Delta V^2}{G}, \quad (1)$$

where  $f$  is a dimensionless factor of order unity that depends on the geometry, inclination, and kinematics of the BLR. The factor  $f$  can in principle be determined for individual AGNs by modeling the BLR (Pancoast et al. 2011, 2014).

At the present time, it is common to use the AGN  $M_{\text{SMBH}}-\sigma_*$  relationship to establish a mean value for this scaling factor; the most recent published value is  $\langle f \rangle = 4.31 \pm 1.05$  for a line dispersion estimate of  $\Delta V$  (Grier et al. 2013a). While use of an average value  $\langle f \rangle$  cannot be expected to yield particularly accurate masses for individual sources, it is useful for application to large data sets.

<sup>1</sup> Department of Astronomy, The Ohio State University, 140 West 18th Avenue, Columbus, OH 43210, USA; yzu@cmu.edu

<sup>2</sup> The Center for Cosmology and Astroparticle Physics, The Ohio State University, 191 West Woodruff Avenue, Columbus, OH 43210, USA

<sup>3</sup> Department of Physics, Carnegie Mellon University, 5000 Forbes Avenue, Pittsburgh, PA 15213

<sup>4</sup> Warsaw University Observatory, Al. Ujazdowskie 4, 00-478 Warszawa, Poland

RM results have also established an empirical relationship between the AGN luminosity  $L$  and the BLR size  $R_{\text{BLR}}$  of the form

$$R_{\text{BLR}} \propto L^\alpha, \quad (2)$$

where  $\alpha \approx 0.5$  (Wandel, Peterson, & Malkan 1999; Kaspi et al. 2000; Kaspi et al. 2005; Bentz et al. 2006, 2009, 2013). This relationship has been independently established through microlensing studies (Guerras et al. 2013). Its particular value is that the AGN luminosity can thus be used as a proxy for measuring the BLR radius, thus bypassing resource-intensive RM.

It is nevertheless desirable in many cases to measure  $R_{\text{BLR}}$  and  $M_{\text{SMBH}}$  directly. However, it is clear that more efficient methods must be found if one wishes to extend RM to higher-redshift, fainter objects. One possibility that is being actively pursued is to use multi-object spectrographs on large telescopes to monitor as many as hundreds of quasars simultaneously (Shen et al. 2015; King et al. 2015). With a large-enough telescope and a wide-enough field of view, the surface density of quasars is high enough to make spectroscopic multiplexing effective.

Another possibility is to make RM measurements with purely photometric data, using either narrow-band (Haas et al. 2011; Pozo Nuñez et al. 2012) or broad-band (Chelouche & Daniel 2012; Chelouche et al. 2012; Edri et al. 2012) filters. The narrow-band approach essentially reduces to the spectroscopic RM problem by subtracting the continuum contribution to the narrow photometric band containing the broad emission line.

However, the broad-band case is considerably more complicated because the emission lines and continuum are not easily separable. In this case the continuum variability has to be carefully modeled or removed statistically. Chelouche & Daniel (2012) developed a method by looking for an excess cross-correlation signal at non-zero time lags between two broad-band light curves and applied it to a subset of the Palomar–Green quasar sample, finding broad agreement with the spectroscopic RM results, albeit with very large uncertainties. The cross-correlation of two bands, one on and one off the line, or the auto-correlation of one band on the line, must mathematically have power near both zero lag due to the correlation of the continuum or line variability with itself and at the emission-line lag due to the cross-correlation between the line and the continuum. This by no means implies the existence of separate peaks, but only that the presence of the line emission leads to a broader correlation function. Chelouche & Zucker (2013, hereafter CZ13) proposed a comprehensive approach based on cross-correlation functions (CCF), which takes into account the continuum time lag between two broad bands and estimates model uncertainties using Monte Carlo simulations. However, discussions of photometric RM to date have not quantitatively addressed the ability to recover lags accurately as a function of line strength, sampling, and signal-to-noise ratio or made detailed comparisons to the performance of spectroscopic RM. Moreover, while the work of CZ13 shows that the existence of a lag can be detected, whether or not it can be measured with sufficient accuracy that the method becomes competitive with spectroscopic RM remains dubious. While

the problems of photometric RM are both fairly obvious and significant, thorough investigation of the technique is warranted since, as pointed out by CZ13, the community will soon be awash in photometric monitoring data on quasars that we must be ready to exploit fully.

Here we consider a somewhat different approach to extracting lags from photometric data alone. A series of recent studies (Kelly et al. 2009; Kozłowski et al. 2010; MacLeod et al. 2010; Zu et al. 2013; Andrae et al. 2013) have shown that quasar optical variability is well modeled by the damped random walk (DRW) stochastic process on time scales from several days to years, although there may be deviations on shorter time scales (Mushotzky et al. 2011; Zu et al. 2013). Zu et al. (2011; hereafter ZKP11) further adapted the DRW model to address RM, where it has several significant advantages over standard methods. First, irregularly sampled light curves require some method of interpolation for any inter-comparison, where the standard approaches use either binning (Edelson & Krolik 1988) or linear interpolation (Gaskell & Sparke 1986). The ZKP11 approach essentially averages over all possible continuous light curves that are statistically consistent with the observed data and the DRW (or other) stochastic process (Rybicki & Press 1992). Second, the means of estimating likelihoods in the various CCF methods are fairly *ad hoc*, while the ZKP11 methods use likelihood functions that can be interpreted using standard Bayesian or frequentist methods. Finally, the approach allows generalizations that can automatically include calibration uncertainties, temporal trends, data correlations or multiple lines or line velocity bins in the full likelihood calculation. We have made the analysis software public<sup>5</sup> and it is increasingly being used in recent RM studies (Grier et al. 2012a,b, 2013b; Dietrich et al. 2012; Zhang 2013; Shapovalova et al. 2013; Li et al. 2013; Shappee et al. 2014). The spectroscopic RM module in the software has also provided important cross-checks to some narrow-filter-based photometric RM studies (e.g., Pozo Nuñez et al. 2013).

For the sake of completeness, we also consider the greater challenge of single-band photometric RM: a reverberating emission line in a photometric band will result in an “echo” of the continuum variations and in principle, if the DRW is indeed a good model for the continuum variability, the emission-line echo should be identifiable, given sufficient high-quality data.

Here we will apply our modeling approach to a comparison of spectroscopic and both two and single-band photometric RM. In particular, we address whether photometric RM is more or less observationally efficient than spectroscopic RM. We will first summarize our approach in §2. In §3, we carry out a series of Monte Carlo simulations for all three approaches as a function of cadence, campaign duration, and line strength relative to the continuum. In §4, we examine two-band photometric RM of PG 0026+129 for which contemporaneous spectroscopic and photometric light curves are available. In §5, we use photometric data on the well-studied Seyfert galaxy NGC 5548 as a second case study. In §6, we examine single-band photometric RM using OGLE (Optical Gravitational Lensing Experiment) quasars behind the

<sup>5</sup> JAVELIN (SPEAR) <http://bitbucket.org/nye17/javelin>

Magellanic Clouds. We summarize our results in §7 and consider the applicability of these methods in large-scale surveys such as LSST.

## 2. METHODOLOGY

In any given photometric band, quasar variability consists of two components, one from the continuum and the other from broad emission lines, plus contaminants such as the host-galaxy flux and narrow emission lines that do not vary on the relevant time scales (e.g., Peterson et al. 2013). We model the continuum variability as a Gaussian process (Rasmussen & Williams 2006; Kelly et al. 2013; Zu et al. 2013)

$$c(t) = \mathcal{GP}\{\bar{c}, \kappa(t, t')\}, \quad (3)$$

where the mean function  $\bar{c}$  is constant and  $\kappa(t, t')$  is the covariance function between two epochs. For the DRW model discussed in §1,  $\kappa(t, t') = \sigma^2 \exp(-|t - t'|/\tau_d)$  where  $\sigma^2$  and  $\tau_d$  are the variance and characteristic time scale of the process. The variability of the broad emission lines relative to the continuum can be described as

$$l(t) = \int \Psi(t - t')c(t) dt', \quad (4)$$

where  $\Psi(t)$  is the transfer function. In this paper we focus on cases in which there is only one dominant broad line or multiple broad lines that have similar lags. In particular, following ZKP11, we explicitly model  $\Psi(t)$  as a top hat transfer function centered on time lag  $\tau$  with width  $w$  and amplitude  $A$ , so that

$$\Psi(t) \equiv \Psi(t|\tau, A, w) = A/w \text{ for } \tau - w/2 \leq t < \tau + w/2. \quad (5)$$

Here we consider two classes of monitoring bands: a continuum band (hereafter referred to as the  $\mathbb{C}$ -band) uncontaminated by lines, and a line band (hereafter referred to as the  $\mathbb{L}$ -band) containing both line and continuum contributions. The light curves in the  $\mathbb{C}$ - and  $\mathbb{L}$ -band light curves are  $f_{cb} = c(t) + u_{cb}$  and  $f_{lb} = \alpha \cdot c(t) + l(t) + u_{lb}$ , respectively, where  $\alpha$  is the ratio between the continuum variabilities in the two bands and  $u_{cb}$  and  $u_{lb}$  represent any contaminating flux from narrow emission lines and the host galaxy. The key problem for photometric RM methods is whether we can distinguish  $l(t)$  from  $c(t)$  without measuring  $l(t)$  directly as is done in spectroscopic RM. Depending on the available data, there are two possible approaches to photometric RM.

- We could have both  $\mathbb{C}$  and  $\mathbb{L}$  bands. In this case, The  $\mathbb{C}$ -band light curve provides an independent constraint on the structure and statistics of the continuum variability. Such a model has six parameters,  $\mathbf{p} \equiv \{\sigma, \tau_d, \tau, w, A, \alpha\}$ , where  $u_{cb}$  and  $u_{lb}$  are nuisance parameters marginalized in the analysis.
- If we have only the  $\mathbb{L}$  band where  $f_{lb}(t) = \alpha \cdot c(t) + l(t) + u_{lb}$ , then the continuum and line variabilities have to be inferred simultaneously. Compared to the two-band model, the number of parameters in the one-band model is fewer ( $\alpha$  is fixed to be unity so that  $\mathbf{p} \equiv \{\sigma, \tau_d, \tau, w, A\}$ ) but the difficulty is substantially increased due to the lack of independent information on the continuum variability as compared to the lines.

We explore both of these approaches using the statistical framework described by ZKP11. Here we briefly summarize this approach, and readers should refer to ZKP11 for additional details.

Let  $\mathbf{y}$  be a vector comprised of all the light curves, either the combined  $\mathbb{C}$ - and  $\mathbb{L}$ -band light curves or the one  $\mathbb{L}$ -band light curve. We model  $\mathbf{y}$  as

$$\mathbf{y}(t) = \mathbf{s}(t) + \mathbf{n} + L\mathbf{q}, \quad (6)$$

where  $\mathbf{s}(t)$  is the underlying variability signal with zero mean (e.g.,  $c(t) - \bar{c}$  in  $\mathbb{C}$ -band) and covariance matrix  $S$ ,<sup>6</sup>  $\mathbf{n}$  is the measurement error with covariance matrix  $N$ , and  $L$  is a  $x \times K$  matrix where  $x$  and  $K$  are the number of light curves and total number of data points in  $\mathbf{y}$ , respectively. In particular, for the two-band model,  $L$  has entries of  $(1, 0)$  for the  $\mathbb{C}$ -band data points, and  $(0, 1)$  for the  $\mathbb{L}$ -band data points, while for the one-band model  $L$  is a vector of all ones. The linear coefficients  $\mathbf{q}$  are the light curve means, including contributions from  $\bar{c}$ , the mean of  $l(t)$ , and the host galaxy light and narrow line flux ( $u_{cb}$  and  $u_{lb}$ ).

As derived by ZKP11, after marginalizing over  $\mathbf{q}$ , the likelihood of the model parameters is

$$\mathcal{L}(\mathbf{y}|\mathbf{p}) = |C|^{-1/2} |L^T C^{-1} L|^{-1/2} \exp\left(-\frac{\mathbf{y}^T C_{\perp}^{-1} \mathbf{y}}{2}\right) \quad (7)$$

where  $C = S + N$  is the overall data covariance and

$$C_{\perp}^{-1} = C^{-1} - C^{-1} L (L^T C^{-1} L)^{-1} L^T C^{-1}. \quad (8)$$

For light curve prediction, the best estimate for the mean intrinsic variability is

$$\hat{\mathbf{s}} = S C^{-1} (\mathbf{y} - L \hat{\mathbf{q}}), \quad (9)$$

where

$$\hat{\mathbf{q}} = (L^T C^{-1} L)^{-1} L^T C^{-1} \mathbf{y} \quad (10)$$

is the best estimate for the light curve means, and the expected variance in the estimated variability about the mean is

$$\langle (\mathbf{s} - \hat{\mathbf{s}})^2 \rangle = S - S^T C_{\perp} S. \quad (11)$$

The only difference between spectroscopic and photometric RM approaches within this framework lies in the computation of the covariance matrix  $S$ . For two-band photometric RM,  $S_{ij}$  involves three types of entries, the DRW covariance function  $\kappa(t_j - t_i)$ , the covariance between  $f_{cb}(t)$  and  $f_{lb}(t)$

$$\langle f_{cb}(t_i) f_{lb}(t_j) \rangle = \alpha \kappa(t_j - t_i) + \alpha \langle c(t_i) l(t_j) \rangle, \quad (12)$$

and the covariance between two  $\mathbb{L}$ -band light curves

$$\langle f_{lb}(t_i) f_{lb}(t_j) \rangle = \alpha^2 \kappa(t_j - t_i) + \alpha \langle c(t_i) l(t_j) \rangle + \alpha \langle l(t_j) c(t_i) \rangle + \langle l(t_i) l(t_j) \rangle, \quad (13)$$

while for the one-band case, only Equation 13 is relevant and we can take  $\alpha \equiv 1$ . For the simple case of top-hat transfer functions, all the terms in Equations 12 and 13 have analytical forms, which can be found in the Appendix of ZKP11.

Following ZKP11, we use MCMC methods to estimate the posterior distributions of model parameters. For

<sup>6</sup> The entries of  $S_{ij}$  are simply the values of the covariance function  $S_{ij} = S(\Delta t_{ij})$ , so we have used the same symbol for both.

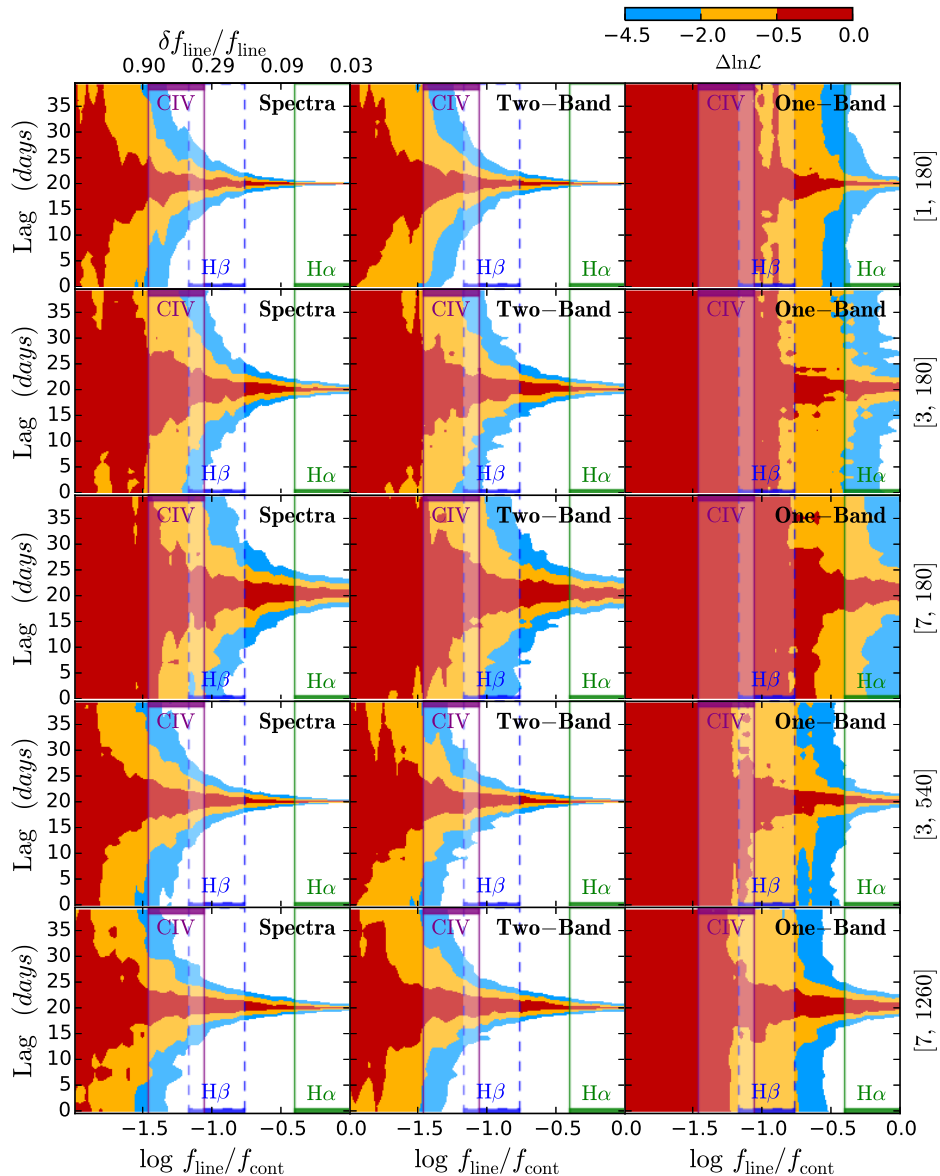


**Figure 1.** Significance of lag detection as function of broad line strength in spectroscopic (left), two-band (middle) and one-band (left) RM. Panels in the same row assume the same cadence and duration, labeled in the format [cadence, duration] on the right of each row. The contours are color-coded by the colorbars shown at top, with the red, yellow, and blue contours roughly corresponding to the  $1\sigma$ ,  $2\sigma$ , and  $3\sigma$  confidence regions for one object, respectively. If one could combine the likelihoods of multiple identical objects in each panel, the corresponding confidence regions for detecting a *mean* lag will shrink considerably. For example, after stacking nine objects the red contours will represent  $3\sigma$  limits instead of  $1\sigma$  ( $\Delta \ln \mathcal{L}$  goes from  $-0.5$  to  $-4.5$ ). There assume 1% measurement uncertainties for the continuum band and the top x-axis for the upper left panel shows the corresponding fractional uncertainties in the spectroscopic line flux. See text for details.

**Table 1**  
Lag Estimates for Simulated H $\beta$  Lines

Cad	Baseline	$N_p$	Spec	Two-band	One-band
1	180	180	$19.4 \pm 2.2$	$20.1 \pm 2.0$	$20.7 \pm 11.3$
3	180	60	$20.2 \pm 5.1$	$20.1 \pm 6.4$	$18.6 \pm 10.8$
3	540	180	$20.3 \pm 2.2$	$19.6 \pm 2.1$	$20.9 \pm 8.0$
7	180	26	$19.2 \pm 6.7$	$17.2 \pm 7.8$	$22.8 \pm 9.2$
7	1260	180	$20.4 \pm 1.6$	$19.8 \pm 1.9$	$21.3 \pm 6.8$

**Note.** — Mean lags and their  $1\text{-}\sigma$  uncertainties for the simulated H $\beta$  lines ( $f_{\text{line}}/f_{\text{line}}=0.1$ ) in Figure 1. “Cad” gives the observing cadence in days over a period of “Baseline” days, producing  $N_p$  epochs of observations. The input lag is 20 days.

the two-band case, we first constrain  $\sigma$  and  $\tau_d$  using

the C-band light curve, and then apply the 68% confidence limit on each of the two parameters as uncorrelated log-normal priors to the second step, in which we derive constraints on all the six parameters using the combined C and L-band light curves. As explained in ZKP11, the uncorrelated log-normal priors on  $\sigma$  and  $\tau_d$  are necessary to exclude a wrong class of solutions with  $\tau_d \rightarrow 0$  during the joint fit, and are much more conservative than the correlated 2D constraints from the C-band light curve. For the one-band case, however, we drop the first step and fit the model to the L-band light curve directly using uniform priors on  $\log \sigma$  and  $\log \tau_d$ . While we do not do so here, a prior on  $A/\alpha$ , the line strength in the band, can be added to “stabilize” the line contribution. The algorithms for the two photomet-

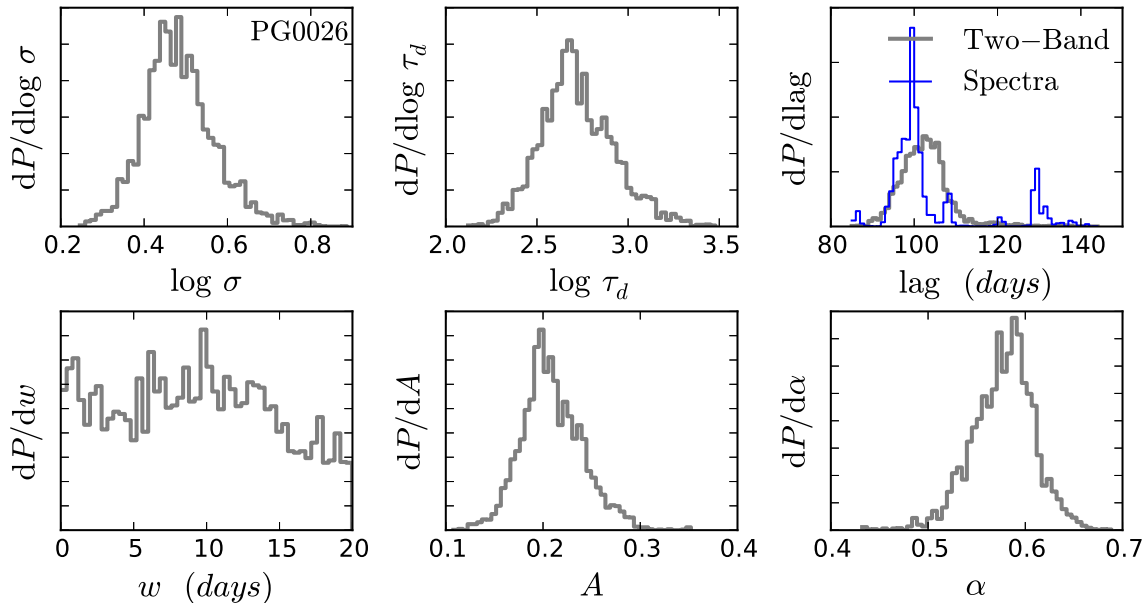


**Figure 2.** Constraints from the photometric RM model using the  $B$ - and  $R$ -band light curves of PG 0026+129 for the DRW parameters  $\sigma$ ,  $\tau_d$ , the lag, the kernel width  $w$ , the transfer function amplitude  $A$ , and the ratio between the continua in the two bands  $\alpha$ . The thin histogram in the top right panel is the estimate of the lag from spectroscopic RM.

ric RM methods are implemented in a new update of the JAVELIN software, which is the updated version of SPEAR released with ZKP11 and is publicly available at <http://bitbucket.org/nye17/javelin>.

### 3. APPLICATION TO SIMULATED LIGHT CURVES

Similar to its spectroscopic counterpart, lag detection in photometric RM is very sensitive to the sampling properties of the light curves, which are mainly characterized by the duration and the cadence of observations. Photometric RM further depends critically on the relative strength of the broad lines compared to the continuum flux within the observational band (hereafter simply referred to as the “line strength”), whereas in spectroscopic RM the separation between line and continuum fluxes is more sensitive to the quality of spectra than to the line strength. However, since photometry is more efficient than spectroscopy in collecting photons (but only by a factor of  $\sim 2$  for modern spectrographs), given fixed sampling conditions and exposure time, photometric RM could be competitive with spectroscopic RM. Spectroscopic RM data are more difficult to calibrate, due to time- and wavelength-dependent slit-losses and variable host galaxy contamination. Photometric RM, on the other hand, is (much) more strongly restricted in the redshift range accessible to an individual observation due to the narrow wavelength coverage of filters as compared to spectrographs.

To obtain a quantitative understanding of the feasibility of photometric lag detection, we modelled the traditional spectroscopic and the two photometric RM methods using mock light curves simulated using the Cholesky decomposition technique described by ZKP11. We considered monitoring baselines of 180, 540, and 1260 days and cadences of 1, 3, and 7 days as a function of the line strength. The line strength  $r$  is characterized by the ratio of line to continuum fluxes in the  $\mathbb{L}$ -band,  $r \equiv \overline{l(t)/c(t)}$ . Note that  $r$  is a function of both the equivalent width

of the line and the transmission curve of the filter. We considered 20 log-spaced values of this ratio from 0.01 to 1.0. For each case we generated 50 random realizations of light curves assuming a typical local Seyfert 1 galaxy at  $z \sim 0$  like NGC 5548 with  $\sigma = 0.2\bar{c}$ ,  $\tau_d = 40$  days,  $\tau = 20$  days, and  $w = 2$  days (cf., Figure 10 in ZKP11). We also include the same constant term  $u$  in both bands, so that the  $\mathbb{C}$ -band light curve is  $f_{cb}(t) = c(t) + u$  and the  $\mathbb{L}$ -band light curve is  $f_{lb}(t) = c(t) + l(t) + u$ . The light curve means are still independently fit even if the input values are the same. For each photometric light curve, we assume a 1% fractional photometric uncertainty in the total band flux (i.e.,  $\bar{c} + u$ ). The impact of any potential deviation from the DRW model on short time scales should be negligible.

For the simulations, we assume that the continuum and host contributions to the two bands are the same and that the host contribution is equal to the mean of the quasar continuum. Thus, if  $\sigma_c$  is the noise in the quasar continuum, the noise in the continuum band ( $c(t) + u$ ) is  $\sigma_{cb} = 2^{1/2}\sigma_c$ , the noise in the line band is  $\sigma_{lb} = (2 + r)^{1/2}\sigma_c$ , and the noise in the line flux after subtracting the continuum and the host is  $\sigma_l = (4 + r)^{1/2}\sigma_c$ , assuming similar width for the two bands. We set the fractional error of the continuum band to  $\sigma_{cb}/(u + \bar{c}) = \sigma_{cb}/2\bar{c} = 2^{-1/2}\sigma_c/\bar{c} = 0.01$ , which means that the fractional error in the spectroscopic line flux is  $\sigma_l/\bar{l} = 0.02(2 + 0.5r)^{1/2}/r$ .

Figure 1 summarizes the results of these simulations, where we show the *average* likelihood ratio  $\ln \mathcal{L}/\mathcal{L}_{\max}$  expected for a single object as a function of the input line strength  $r$  and the output lag estimate  $\tau$  for the spectroscopic (left column), two-band photometric (middle column), and one-band photometric (right column) methods. The typical ranges of  $r$  for the C IV H $\beta$  and H $\alpha$  lines and typical broad band filters are indicated by the vertical bands. These were estimated by convolving the composite quasar spectrum from Vanden Berk et al.

(2001) with the transmission curves of typical broad band photometric systems (e.g., SDSS or Johnson bands). To avoid clutter, we do not show the  $r$  range for the MgII line. It would lie between the ranges for C IV and H $\beta$ .

The top three panels in Figure 1 show the forecasts for our fiducial monitoring campaign — daily cadence over one observing season (i.e., six months). The mock light curves used for the second and third rows have lower sampling rates, with 3 and 7-day cadences, respectively, while having the same overall temporal baseline as the fiducial campaign. The mock light curves used for the fourth and fifth rows have lower sampling rates but longer baselines, maintaining the same number of epochs (180) as in the first test (the top row). Unsurprisingly, for any given sampling of the light curves (i.e., comparing panels in the same row), spectroscopic RM performs better than the two-band photometric RM, and both of them are significantly better than the one-band photometric RM. Table 1 summarizes the result for  $r=1$  (H $\beta$ ). For example, the lag estimates for the fiducial campaign are  $19.4 \pm 2.2$ ,  $20.1 \pm 2.0$ , and  $20.7 \pm 11.3$  days for the spectroscopic, two-band, and one-band photometric RM cases. For this strong line, the two-band approach is competitive with spectroscopy, but the one-band approach is not. Within each method (i.e., comparing panels in the same column), the lag detection efficiency is very sensitive to the cadence for any fixed baseline, but largely due to the decrease in the number of data points for longer cadences — the difference among the first, the fourth, and the bottom panels in each column, where the total number of epochs is fixed to 180, is much smaller than that among the top three panels where the number of epochs is varied. In particular, in the middle column for the two-band test, the fiducial and the two long-baseline tests (bottom two panels) yield very similar lags of  $20 \pm 2$  days for lines with  $r = 0.1$ , while the two short-baseline tests (second and third panels) find  $20 \pm 6$  days or worse, respectively. However, we expect the uncertainties in the lag estimates to rise rapidly even for a fixed number of epochs as the sampling rate decreases once the cadence is larger than 20 days.

The uncertainties in the lags are also highly sensitive to the magnitude of the line contribution in the photometric band. As can be seen in Figure 1, this means that for campaigns with 180 epochs, H $\alpha$  lags are almost always measurable with high significance using photometric RM methods, H $\beta$  lags are only marginally measurable, and the MgII and C IV lags are never measurable for light curves with similar sampling properties and physical parameters. Single-band RM is very challenging even for H $\alpha$  and relatively “narrow” broad-band filters such as the SDSS system (Fukugita et al. 1996).

#### 4. CASE STUDY I: TWO-BAND PHOTOMETRIC RM OF PG 0026+129

The best chance of obtaining robust photometric lags is to focus on quasars whose H $\alpha$  line lies within one passband and the continuum is clearly observed in another passband. The Palomar–Green (PG) quasar light curves from Giveon et al. (1999) consist of two-band ( $B$  and  $R$ ) light curves of 42 quasars from the PG sample, with typical cadences of  $\sim 20$  or 40 days over a seven-year time span and an average photometric uncertainty of 0.017 mag. The sample

has a redshift range of  $0.1 \lesssim z \lesssim 0.3$ , making the  $B$  and  $R$ -band light curves suitable for detecting H $\alpha$  lags using two-band photometric RM (with  $B$  being the C-band and  $R$  being the L-band). Many of these targets were also contemporaneously monitored in order to make spectroscopic RM measurements (Kaspi et al. 2000). For these objects, we can assess the performance of photometric RM by comparing the photometric lag constraints to the corresponding results using spectroscopic RM. Therefore, we focus on seven objects — PG 0026+129, PG 0052+251, PG 0804+761, PG 0844+349, PG 1613+658, PG 1617+175, and PG 2130+099 — that are both photometrically better sampled (i.e., 20-day cadence) and have spectroscopic H $\alpha$  light curves. Chelouche & Daniel (2012) also made photometric RM measurements for several of these systems but with such large uncertainties ( $\sim 100$  to 200 days) that the significance of any comparison is very small.

In each case, we model the continuum-band light curve as  $f_{cb}(t) = c(t)$  and the line-band light curves as  $f_{lb}(t) = \alpha \cdot c(t) + \Psi(t) * c(t)$  where  $\Psi(t)$  is the top-hat transfer function centered on lag  $\tau$  with width  $w$  and amplitude  $A$  (Equation 5), and  $\alpha$  scales the continua between the two bands. For better consistency in the modeling of continuum variability, we re-calculated the spectroscopic lags with JAVELIN as described by Zu et al. (2011) using the original Kaspi et al. (2000) light curves. The two methods are largely consistent with each other, with lag differences smaller than twice the average temporal sampling (i.e.,  $2 \times 20$  days) in all cases except PG 1613+658. The cause for the discrepancy in PG 1613+658 is unclear, as the observed  $R$ -band light curve simply cannot be matched by the prediction from JAVELIN using the spectroscopic H $\alpha$  lag.

We applied our two-band photometric RM analyses to all seven of these quasars. Unfortunately, all of the cases proved to be somewhat problematic, usually because of the low amplitude of H $\alpha$  variability, but for other reasons as well (e.g., the original lags for PG 2130+099 were badly misidentified; see Grier et al. 2008; Grier et al. 2012b).

Only PG 0026+129 yielded a plausible result. Figure 2 shows the posterior probability distributions for the six parameters in the two-band photometric RM model for PG 0026+129. The distribution of the top-hat width  $w$  is mostly flat within 20 days, which is the sampling interval of the light curves. The thin blue histogram in the top right panel shows the posterior probability distribution of the H $\alpha$  lag inferred from spectroscopic RM. The lag constraints from the two RM methods agree with each other well, indicating that the photometric RM approach is capable of separating the H $\alpha$  signals from the continuum variability while recovering the correct lag. The ratio of  $A$  to  $\alpha$  indicates that the line variability is roughly 1/3 of the continuum variability within the  $R$ -band, also consistent with what we expect for H $\alpha$  based on the spectral template from Vanden Berk et al. (2001).

One virtue of JAVELIN is that it produces an explicit model for the mean and dispersion of the light curves constrained by the data given the best-fitting parameters, as shown in Figure 3. In each panel the observed light curves are shown by the data points with error-

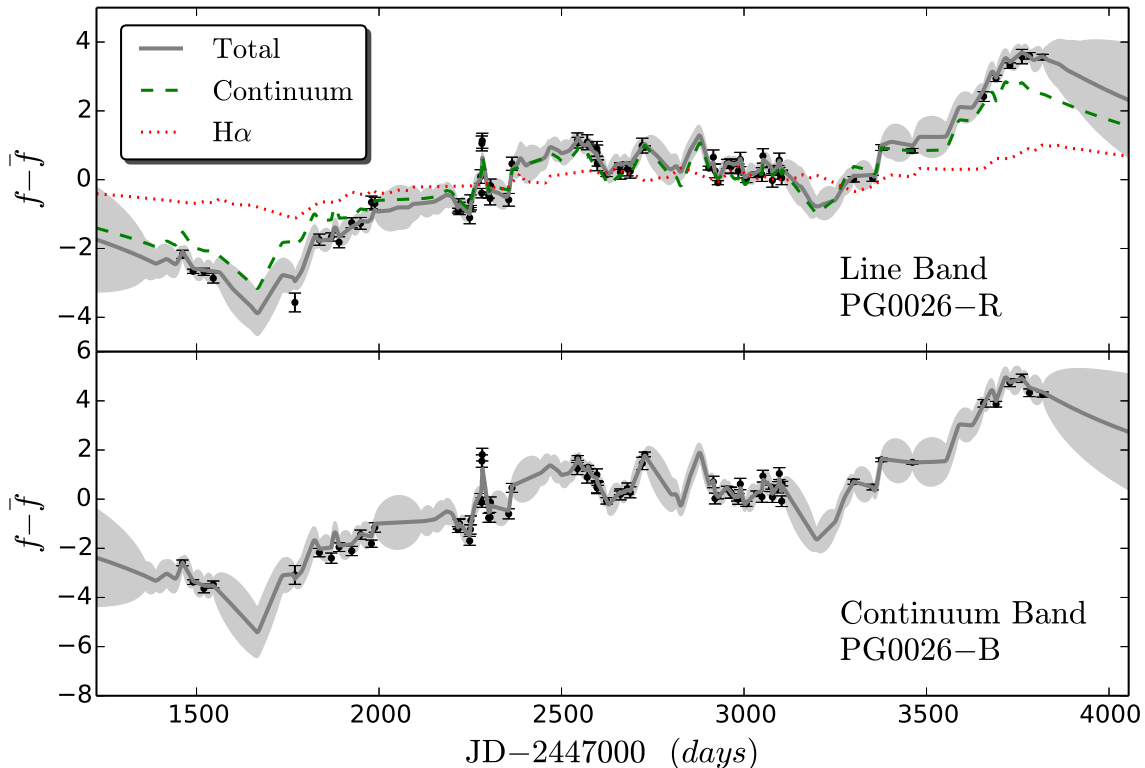


**Figure 3.** Comparison between the data and the mean of the predicted light curves for PG 0026+129, using the best-fitting parameters from Figure 2. The lower panel shows the average of the DRW light curves matching the continuum light curve for the best-fit parameters and the rms scatter of these light curves. The upper panel shows the resulting fits to the line band, as well as the decomposition into the H $\alpha$  line and continuum contributions.

bars, while the solid line and the error “snake” are the estimated mean of light curves consistent with the data and their variance, respectively (Equations 9 and 11). We also show the decomposition of the model for the  $R$ -band light curve into the line and continuum contributions, as shown in the top panel, where the dashed and dotted curves indicate the expected fluxes contributed by the continuum and H $\alpha$  line, respectively. It shows unambiguously that the difference between the  $B$ - and  $R$ -band light curves can be well described by a weaker but lagged version of the  $B$ -band light curve representing the H $\alpha$  light curve.

#### 5. CASE STUDY II: PHOTOMETRIC OBSERVATIONS OF NGC 5548

As previously noted, CZ13 proposed a modified CCF-based photometric RM method for simultaneously estimating the intra-band and line lags. The CZ13 method describes the  $L$ -band light curve as the sum of two scaled and lagged versions of the  $C$ -band light curve with a non-negligible lag between the continua in the two optical bands and a delta function for the transfer function of the line. CZ13 searched through the 3-parameter space (intra-continuum band lag, line lag, and the line-to-continuum flux ratio) for the model which maximizes the correlation coefficient  $R$  between the observed and predicted  $L$ -band light curves. Aside from assuming different models for the  $L$ -band light curve, the two key differences between the CZ13 method and JAVELIN are:

- In order to predict the  $C$ -band light curve values at unobserved epochs, CZ13 employs linear interpola-

tion rather than interpolating in a manner consistent with the underlying process.

- To characterize the uncertainties in their parameter estimates, CZ13 generate a sample of mock light curves as the sum of the data light curves and Gaussian random deviates with the estimated uncertainties as the dispersions, and then infer the parameters for each mock data set to compute the error distributions. JAVELIN employs a MCMC Bayesian approach that is self-consistent within the underlying statistical framework.

To compare the performance of the CZ13 method and JAVELIN we applied both methods to the two-band ( $V$  and  $R$ ) light curves of NGC 5548 from Sergeev et al. (2005) that CZ13 used as their principal example. While there is no H $\alpha$  light curve for this period, NGC 5548 is sufficiently well-characterized that the H $\alpha$  lag can be estimated from the AGN luminosity. NGC 5548 was at a near-historic low-luminosity state at the time of the Sergeev et al. (2005) observations (2001–2002; see Figure 1 in Peterson et al. (2013) for an NGC 5548 continuum light curve over the past two decades). The LAMP spectroscopic RM campaign in 2008, when the continuum was at a similarly low level, yielded lags for H $\beta$  and H $\alpha$  of  $4.25^{+0.88}_{-1.33}$  days and  $11.02^{+1.27}_{-1.15}$  days, respectively (Bentz et al. 2010). Thus, we expect a similar H $\alpha$  lag at the time of the Sergeev et al. (2005) observations.

The results of our analysis of the NGC 5548 photometry are shown in the left panels of Figure 4, where the top panel compares the two inferred lag distributions and the

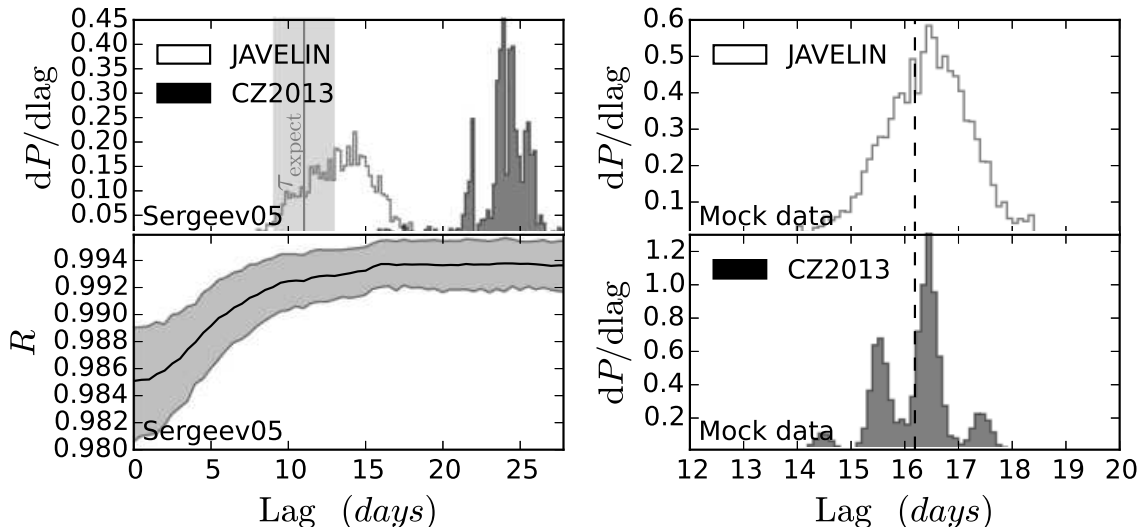


**Figure 4.** Comparison between the JAVELIN and the CCF-based method of CZ13, using the NGC 5548 light curves from Sergeev et al. 2005 (left) and mock light curves (right). The vertical band in the upper left panel indicates the expected lag given the luminosity state of NGC 5548 at the time of observation. See text for details.

bottom panel shows CZ13’s correlation coefficient  $R$  as a function of lag using the best-fitting CZ13 model found at fixed lag. JAVELIN yields a lag of  $\sim 14$  days for  $H\alpha$ , in excellent agreement with the luminosity-based prediction. The CZ13 method yields a lag  $\sim 24$  days, in poor agreement with both the predicted value and the JAVELIN result. We note, however, that our result using the CZ13 method agrees with the estimate in Figure 7 of CZ13, showing peaks at  $> 20$  days, but lag estimates quoted in their Table 1 are smaller and in better agreement with both the predicted lag and the JAVELIN measurement. The discrepancy between the CZ13 and JAVELIN estimates of the  $H\alpha$  lags can be largely attributed to the different interpolation schemes, modulo the difference in assumed transfer functions.

The significance of the CZ13 lag detection is illustrated by the  $R$  curve in the bottom left panel of Figure 4, with the gray band indicating the 68% uncertainty range in  $R$  derived by bootstrapping the light curve data following their procedures. Since the line-band flux is always dominated by the continuum,  $R$  is strong even at zero lag ( $\bar{R}_0 = 0.985$ ), and gradually increases until hitting a plateau at  $\sim 10$  days. Therefore, although the lag distribution derived by CZ13 is longer than 20 days, the statistical significance of the long lags is barely higher than for 10–20-day lags.

Apart from having a shift in the estimated central lags, the two lag distributions in the top left panel of Figure 4 also have different shapes, with a continuous, quasi-normal distribution for JAVELIN and a discrete array of sharp peaks for the CZ13 method (it is unclear whether the lag distribution derived by CZ13 has this spiky feature due to their large temporal bins). To investigate the origin of these differences, we simulated 5000 sets of two-band photometric light curves that have the same sampling and error properties as the NGC 5548 light curves using parameters of  $\sigma = 0.1\sqrt{f_B}$ ,  $\tau_d = 566.2$  days,  $\tau = 16.2$  days,  $w = 2.0$  days,  $A = 0.5$ , and  $\alpha = 0.64$ . To eliminate any discrepancies caused by assuming a different transfer function width  $w$  and intra-band lag, we choose not to

use the best-fitting parameters from the left panel, which prefers a larger  $w$  and a shorter  $\tau$ , and we impose zero lag between the continua in the two broad bands. For each set of the mock light curves, we compute lag distributions from the 5000 experiments for each of the two methods. The results are shown in the two right panels of Figure 4, where the two lag distributions recover the input 16.2-day lag (vertical dashed line) but the shape difference persists. As expected, the lag distribution derived from JAVELIN in the top right panel is continuous and resembles the distribution we see in the top left panel for the data. For the CZ13 test, a close examination of the pattern in the bottom right panel reveals that the discrete peaks occur half-way between integer-day lags while the distribution is heavily suppressed at integer day lags. This peculiar pattern is a numerical artifact caused by the use of linear interpolation and a  $w = 0$  transfer function (i.e., a  $\delta$  function) in the CZ13 method. The Sergeev et al. (2005) observations were obtained on a nightly cadence and we reproduced that cadence for the mock light curves, so no interpolation is required at integer lags to calculate the correlation coefficient  $R$ . At half-integer day lags, the linear interpolation acts like a transfer function with  $w = 1$  day instead of  $w = 0$ , smoothing the light curve, and producing a better correlation by (essentially) reducing the fluctuations due to noise. This problem becomes worse when the quasar variability has a short characteristic time scale compared to the sampling cadence and linear interpolation becomes an increasingly poor approximation. We think this problem is intrinsic to the method, but the binning of the lag probability distribution in CZ13 (their Fig. 7) does not allow us to cross check this issue against their results. We note, however, the instability of measuring short delays ( $\sim 1$  day) between two broad-band continua (or equivalently the lack of robustness in small inter-band delay uncertainties), is a well-known problem in determining gravitational lens time delays (e.g., see Tewes et al. 2013) even for light curves far superior to those used here.

## 6. CASE STUDY III: SINGLE-BAND OGLE QUASAR LIGHT CURVES

The simulations in §3 demonstrate that while it is possible to measure  $H\alpha$  lags using single-band photometric RM, the light curves have to be densely sampled with small photometric uncertainties over a long baseline. Currently one of the best data sets of single-band light curves is from the OGLE experiment<sup>7</sup>, where quasars behind the Small and the Large Magellanic Clouds (SMC and LMC) have been monitored with a  $\sim 2$  day cadence for over 8 yrs in the  $I$ -band by OGLE-III (Udalski et al. 2008) and for  $\sim 2.5$  years by OGLE-IV (Soszyński et al. 2012; Kozłowski et al. 2013b). Most of these quasars were identified by Kozłowski et al. (2011, 2012, 2013a) in part from candidates variability-selected using the DRW model (Kozłowski et al. 2010). As a test application of the one-band photometric RM method, we selected 34 quasars that have prominent, broad  $H\alpha$  emission lines that lie in the  $I$ -band, relatively strong variability, and at least 400 epochs in OGLE-III. Each quasar also has a shorter light curve from OGLE-IV ( $\sim 350$  epochs). We do not combine the two OGLE campaigns for the same object, but derive two lags separately as a means of checking the results. The typical photometric uncertainties of the light curves are  $\sim 0.02$ – $0.04$  mag.

The left column of Figure 5 shows the lag distributions derived by applying the one-band photometric RM to the OGLE-III and IV light curves for five random quasars in the sample. In each panel, dark and light histograms on the left show the constraints from the OGLE-III and IV light curves, respectively. The quasars are expected to have  $H\alpha$  lags of roughly 200–300 days based on their optical luminosity (i.e., estimated by assuming a typical quasar spectrum normalized by the  $I$ -band absolute magnitude using the scaling relations in MacLeod et al. 2010). The five objects all have peaks in their lag distributions between 200–300 days, however, none of them show consistent lag constraints between the two OGLE campaigns. The rest of the quasars in the sample all exhibit similar inconsistencies, indicating that the OGLE light curves collected to date are still insufficient for doing one-band photometric RM, despite the long baseline and high cadence.

The non-detection is likely caused by the relatively large photometric uncertainties compared to the line variability signal. To test the feasibility of one-band photometric RM given OGLE’s sampling rates and photometric errors, we generated two sets of mock light curves that have exactly the same sampling epochs as object MQS J044125.27-702310.5 (top left panel of Figure 5) using  $\sigma = 0.1\bar{f}_I$ ,  $\tau_d = 350$  days,  $\tau = 250$  days,  $w = 9$  days, and  $A = 0.3$ . In one case, we used the original average photometric error of 0.021 mag and in the other we used half this average error (i.e., 0.011 mag). We then repeated the analyses for both sets of mock light curves with the results shown in the middle and right columns of Figure 5, where the input lag is indicated by the vertical dashed line in each panel. The probability distributions in the middle column derived from the mock light curves look less “spiky” than those derived from the data light curves

in the left column, possibly because our mock light curves ignore the flux contributions from broad lines other than  $H\alpha$ . Nonetheless, the one-band RM method fails to detect the  $H\alpha$  lags for the mock light curves with the same photometric errors as the OGLE data, but unambiguously recovers the input lags in all five cases after the photometric uncertainties are reduced by half, as shown in the right column of Figure 5. Therefore, the key problem for one-band photometric RM is that it needs very high-precision photometry compared to what is usually obtained for typical sources in large-scale variability surveys.

## 7. CONCLUSIONS

We have developed a stochastic modeling approach to analysis of photometric RM using the statistical framework introduced by ZKP11, assuming the continuum variability is described by a DRW model and the line transfer function is a top hat. The approach can be applied either for two-band photometric RM, where there is a line band and an independent continuum band, or to one-band photometric RM, where there is only a line band.

By applying the spectroscopic and the two- and one-band photometric RM methods to a suite of simulated light curves, we find that two-band photometric RM can be competitive with spectroscopic RM only for strong (large equivalent width) lines like  $H\alpha$  and  $H\beta$  in terms of lag detection efficiency for fixed sampling conditions. The one-band method, however, requires light curves of much higher photometric quality than is generally achieved and is thus very challenging for any line. For all three methods we also find that when the average sampling interval is smaller than the lag, the lag detection significance is most sensitive to the total exposure time accumulated over all the monitoring epochs and almost independent of cadence.

Application to test cases show that the photometric and spectroscopic lag estimates are broadly consistent with each other and have comparable lag uncertainties. We also used the one-band photometric RM approach to analyze a sample of variable OGLE quasars with strong  $H\alpha$  emission. The lag estimates from separately analyzing the OGLE-III and OGLE-IV light curves generally do not agree. One-band RM fails even for the quasars with some of the best-existing long-term light curves. Simulations show that the problem is that the 0.02–0.04 mag photometric uncertainties of the OGLE quasar light curves are simply too large, but that the one-band method may succeed if the uncertainties were reduced to  $\sim 0.01$  mag. Single-band RM is likely most promising for computing average lags for samples of quasars with similar physical properties (e.g., luminosity) rather than for individual objects.

In our simulations, we find that for the same observing cadence, two-band photometric RM requires measurement uncertainties  $\xi = 0.85$  times smaller than spectroscopic RM to measure a lag with the same accuracy. A common argument for photometric RM is that it requires far less telescope time, so it is interesting to examine this claim quantitatively. Let  $t_0$  be the time required to reach a given signal-to-noise level with a spectrograph that has the efficiency of an imager. Spectrographs are less effi-

<sup>7</sup> There are still better, regular light curves of small numbers of AGNs (e.g., Mushotzky et al. 2011), but the broad *Kepler* filter bandpass makes it poorly suited to this problem.

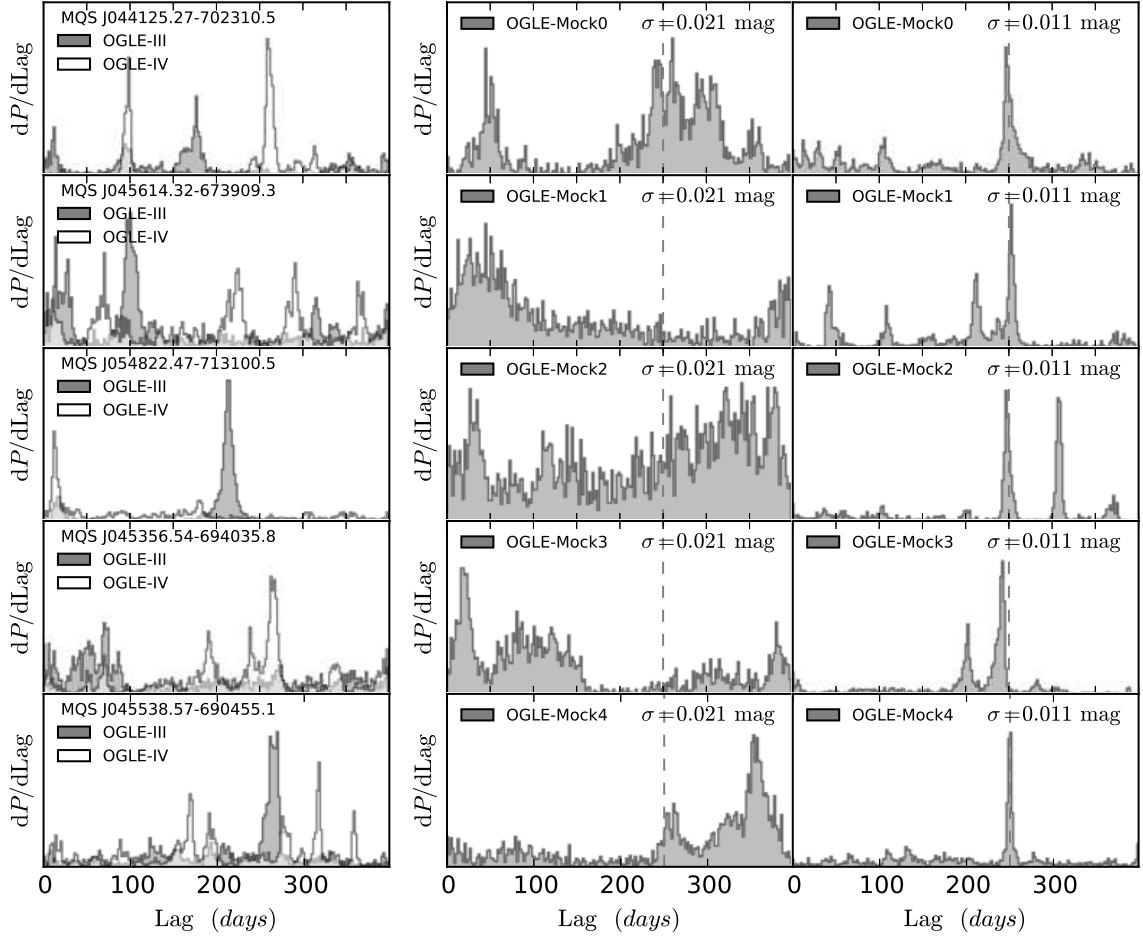


**Figure 5.** Lag estimates from one-band photometric RM, using either the OGLE-III or OGLE-IV light curves (left), mock light curves using the original photometric uncertainties (middle) and half these photometric uncertainties (right). In the panels using mock data, the input lag is indicated by the vertical dashed line.

cient than imagers<sup>8</sup>, and the difference for modern low-resolution spectrographs is a factor of  $\epsilon^{-1} \sim 2$ . Thus, the actual integration time required for spectroscopic RM is  $t_S = \epsilon^{-1}t_0$ . Two-band photometric RM requires two images and requires exposure times of  $\xi^{-2}$  longer because higher signal-to-noise ratio data are required to achieve the same lag precision, leading to a total integration time of  $t_I = 2\xi^{-2}t_0$ . Thus, the ratio of the required integration times is  $t_I/t_S = 2\epsilon\xi^{-2} \approx 1.48$ . Thus, the advantage of two-band photometric RM over spectroscopy is by no means obvious. Adding target acquisition times may ultimately favor imaging because of more demanding telescope pointing requirements for spectroscopy, but only because smaller telescopes have not adequately invested in minimizing such overheads. Other considerations are that spectra are more difficult to calibrate due to variable slit-losses and host contamination, while photometric filters strongly restrict the accessible redshift range per observation compared to spectroscopy.

The conclusion that there is no particular benefit to photometric RM over spectroscopic RM for a single object contradicts a growing “conventional wisdom”. The

issue is that conventional wisdom is based on the integration times that spectroscopic RM campaigns actually use compared to imaging integration times rather than the integration time they could get away with if all that is desired is an average lag. For the latter purpose, spectroscopic RM campaigns are grossly over-integrating, in large part because their present day goals are focused on measuring lags as a function of velocity within the line (Denney et al. 2009; Bentz et al. 2010; Grier et al. 2013b). The real potential gain for photometric RM is that wide-field imaging may allow the measurement of lags for many objects in parallel, but even there, the advantage does not trivially lie with imaging — as noted earlier, pilot RM programs (Shen et al. 2015; King et al. 2015) are already being pursued with wide-field spectrographs like SDSS/BOSS (Dawson et al. 2013) or AAT/AAOmega (Sharp et al. 2006) that are better matched to the surface density of quasars on the sky than are existing wide-field imagers.

The problem with using wide-field spectrographs for RM is largely sociological — in any form, RM requires a large commitment of telescope time, regardless of the size of the telescope, and competition for large, wide-field telescopes is fierce. In contrast, there are imaging telescopes dedicated to photometric surveys, including monitoring programs

<sup>8</sup> Aside from less photon-collecting efficiency, further disadvantages of spectrographs include slit-loss and the high S/N required for the measurements of narrow [OIII] lines used for internal photometric calibrations.

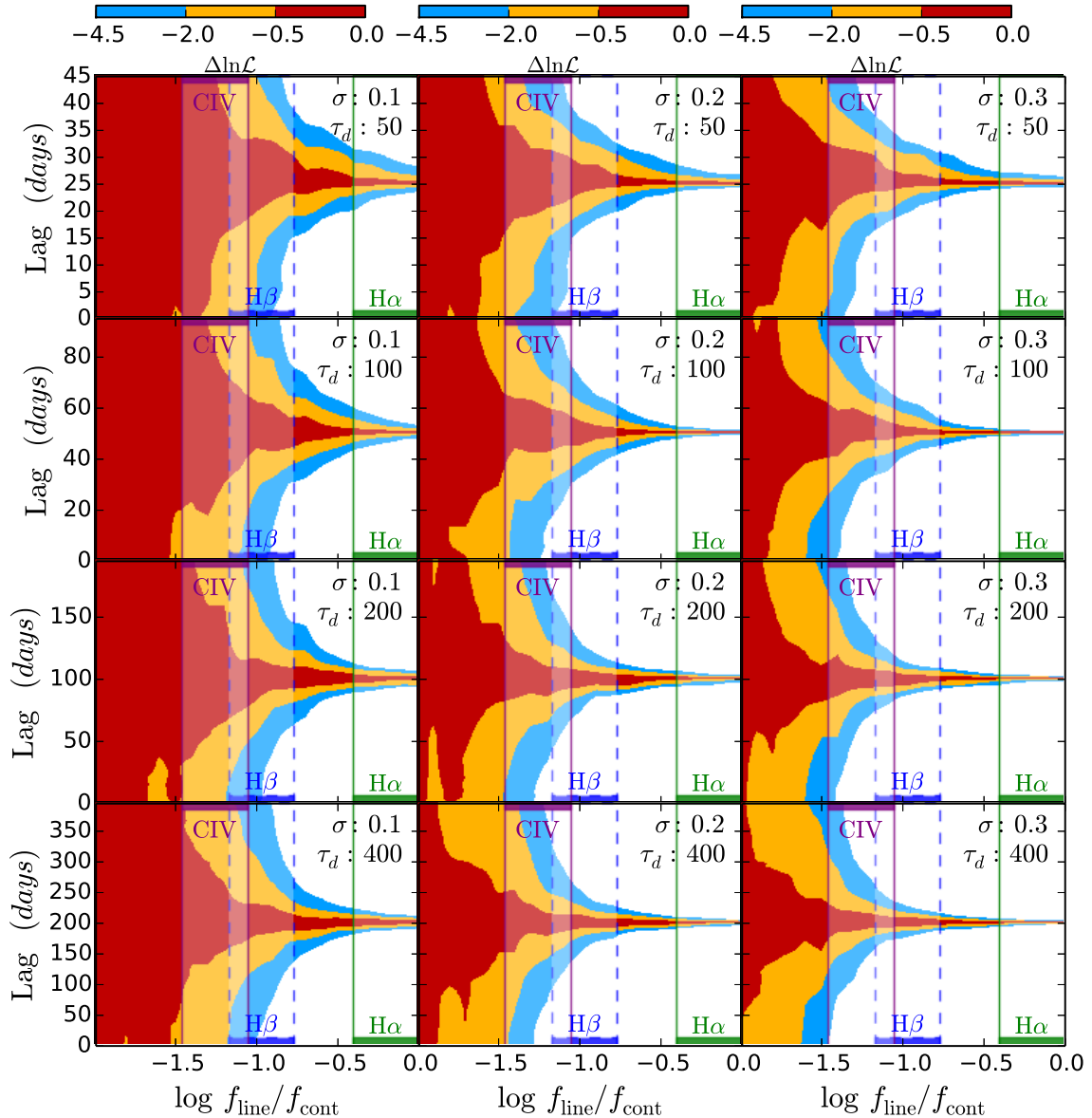


**Figure 6.** As in Figure 1, but for two-band RM using simulated LSST quasar light curves. The variability parameters  $\sigma$  and  $\tau_d$  are listed on the top right of each panel, in units of mag and days, respectively, and we set the input lag to be  $0.5\tau_d$ . All the simulated light curves have 200 epochs, sampled on a 14-day cadence over 10 years. The photometric uncertainties in the continuum band are again 1%.

such as DES (The Dark Energy Survey Collaboration 2005), Pan-STARRS (Kaiser et al. 2002), and ultimately LSST (LSST Science Collaboration 2009). LSST will monitor millions of quasars in six filters over a ten-year baseline, with 200 visits per filter each year. Figure 6 shows the expected lag detection significance for two-band RM using simulated LSST light curves (14-day cadence with 1% photometric uncertainties) using quasar variability parameters of  $\sigma = 0.1, 0.2,$  and  $0.3$  mag and DRW time scales of  $\tau_d = 50, 100, 200,$  and  $400$  days. In each panel, we set the input lag to be  $0.5\tau_d$ , which can always be robustly measured for H $\alpha$  using LSST. The H $\beta$  lags can only be measured within 10% for light curves with  $\sigma > 0.2$  mag and lag  $> 100$  days, while the CIV signals are still too weak to detect. However, since the JAVELIN method is based on likelihoods, unlike the CCF methods proposed by Fine et al. (2012, 2013), it is straightforward to multiply the likelihoods of indi-

vidual quasars to calculate an average lag for quasars of similar luminosity and redshift, which according to the luminosity–radius relation (Equation 2) should share similar emission line lags. For example, we can multiply the H $\beta$  or CIV lag likelihood functions of LSST quasars in the same bin of redshift and luminosity and calculate an average lag for that bin. In some sense, this is what we see in Figures 1 and 6, which show the average likelihoods expected for a single quasar — the combined likelihood for 9 similar quasars would be the same distribution after multiplying the likelihood ratios by 9 with consequent narrowing of the confidence regions, so that the red contours in Figure 1 and 6 would approximately represent  $3\sigma$  confidence regions ( $\Delta \ln \mathcal{L} = -4.5$ ) instead of  $1\sigma$  ( $\Delta \ln \mathcal{L} = -0.5$ ). This composite photometric RM method will be particularly useful for “piggybacking” on surveys that produce a large number of under-sampled quasar light curves. Therefore, provided the systematic

errors in photometry can be controlled to the sub-0.01 mag level, we expect that the number of RM systems will grow dramatically with the incoming high-quality photometric quasar light curves in the near future.

#### ACKNOWLEDGEMENTS

We thank the second referee for helpful comments that have greatly improved the manuscript. We thank Kelly Denney, Stephan Frank, Catherine Grier, Matthias Dietrich, Jan Skowron, and Richard Pogge for many helpful discussions. YZ is supported by an OSU Distinguished University Fellowship, CSK is supported by NSF Grant AST-1009756, SK is supported from (FP7/2007-2013)/ERC grant agreement no. 246678 awarded by the European Research Council under the European Community's Seventh Framework Programme to the OGLE project, and BMP is supported by NSF grant AST-1008882.

#### REFERENCES

- Andrae, R., Kim, D.-W., & Bailer-Jones, C.A.L. 2013, *A&A*, 554, 137
- Barth, A.J., Bennert, V.N., Canalizo, G., et al. 2015, *ApJS*, 217, 26
- Bentz, M.C., Denney, K.D., Grier, C.J., et al. 2013, *ApJ*, 767, 149
- Bentz, M.C., Peterson, B.M., Pogge, R.W., Vestergaard, M., & Onken, C.A. 2006, *ApJ*, 644, 133
- Bentz, M. C., Peterson, B. M., Netzer, H., Pogge, R. W., & Vestergaard, M. 2009, *ApJ*, 697, 160
- Bentz, M.C., Walsh, J.L., Barth, A.J., et al. 2010, *ApJ*, 716, 993
- Blandford, R.D., & McKee, C.F. 1982, *ApJ*, 255, 419
- Carnall, A.C., Shanks, T., Chehade, B. et al. 2015, *MNRAS*, 451, L16
- Chelouche, D., & Daniel, E. 2012, *ApJ*, 747, 62
- Chelouche, D., Daniel, E., & Kaspi, S. 2012, *ApJ*, 750, L43
- Chelouche, D., & Zucker, S. 2013, *ApJ*, 769, 124
- The Dark Energy Survey Collaboration, 2005, [arXiv:astro-ph/0510346](http://arxiv.org/abs/astro-ph/0510346)
- Dasyra, K.M., Tacconi, L.J., Davies, R.I., et al. 2007, *ApJ*, 657, 102
- Dawson, K.S., Schlegel, D.J., Ahn, C.P., et al. 2013, *AJ*, 145, 10
- Denney, K.D., Peterson, B.M., Pogge, R.W., et al. 2009, *ApJ*, 704, L80
- Denney, K.D., Peterson, B.M., Pogge, R.W., et al. 2010, *ApJ*, 721, 715
- De Rosa, G., Peterson, B.M., Ely, J., et al. 2015, *ApJ*, 806:128
- De Rosa, G., Venemans, B.P., Decarli, R., et al. 2014, *ApJ*, 790:145
- Di Matteo, T., Colberg, J., Springel, V., Hernquist, L., & Sijacki, D. 2008, *ApJ*, 676, 33
- Di Matteo, T., Springel, V., & Hernquist, L. 2005, *Nature*, 433, 604
- Dietrich, M., Peterson B.M., Grier, C.J., et al. 2012, *ApJ*, 757, 53
- Edelson, R. A., & Krolik, J. H. 1988, *ApJ*, 333, 646
- Edri, H., Rafter, S.E., Chelouche, D., Kaspi, S., & Behar, E. 2012, *ApJ*, 756, 73
- Fabian, A.C. 1999, *MNRAS*, 308, L39
- Ferrarese, L., & Merritt, D. 2000, *ApJ*, 539, L9
- Ferrarese, L., Pogge, R.W., Peterson, B.M., et al. 2001, *ApJ*, 555, L79
- Fine, S., Shanks, T., Croom, S.M., et al. 2012, *MNRAS*, 427, 2701
- Fine, S., Shanks, T., Green, P., et al. 2013, *MNRAS*, 434, L16
- Fukugita, M., Ichikawa, T., Gunn, J.E., et al. 1996, *AJ*, 111, 1748
- Gaskell, C. M., & Sparke, L. S. 1986, *ApJ*, 305, 175
- Gebhardt, K., Bender, R., Bower, G., et al. 2000, *ApJ*, 543, L5
- Giveon, U., Maoz, D., Kaspi, S., Netzer, H., & Smith, P. S. 1999, *MNRAS*, 306, 637
- Graham, A.W., Onken, C.A., Athanassoula, E., & Combes, F. 2011, *MNRAS*, 412, 2211
- Grier, C.J., Martini, P., Watson, L.C., et al. 2013a, *ApJ*, 773:90
- Grier, C.J., Peterson, B.M., Bentz, M.C., et al. 2008, *ApJ*, 688, 837
- Grier, C.J., Peterson, B.M., Horne, K., et al. 2013b, *ApJ*, 764:47
- Grier, C.J., Peterson, B.M., Pogge, R.W., et al. 2012a, *ApJ*, 744, L4
- Grier, C.J., Peterson, B.M., Pogge, R.W., et al. 2012b, *ApJ*, 755, 60
- Guerras, E., Mediavilla, E., Jimenez-Vicente, J., Kochanek, C.S., Muñoz, J.A., Falco, E., & Motta, V. 2013, *ApJ*, 764:160
- Haas, M., Chini, R., Ramolla, M., Pozo Nuñez, F., et al. 2011, *A&A*, 535, 73
- Jiang, L., McGreer, I.S., Fan, X., et al. 2015, *AJ*, 149:188
- Kaiser, N., Aussel, H., Burke, B.E., et al. 2002, in *Proceedings of the SPIE*, 4836, 154
- Kaspi, S., Maoz, D., Netzer, H., et al. 2005, *ApJ*, 629, 61
- Kaspi, S., Smith, P.S., Netzer, H., et al. 2000, *ApJ*, 533, 631
- Kelly, B.C., Bechtold, J., & Siemiginowska, A. 2009, *ApJ*, 698, 895
- Kelly, B.C., Treu, T., Malkan, M., Pancoast, A., & Woo, J.-H. 2013, *ApJ*, 779:187
- King, A. 2003, *ApJ*, 596, L27
- King, A. 2005, *ApJ*, 635, L121
- King, A., Martini, P., Davis, T.M., et al. 2015, *MNRAS*, in press ([arXiv:1504.03031](http://arxiv.org/abs/1504.03031))
- Kozłowski, S., Kochanek, C.S., Jacyszyn, A.M., et al. 2012, *ApJ*, 746:27
- Kozłowski, S., Kochanek, C.S., & Udalski, A. 2011, *ApJS*, 194, 22
- Kozłowski, S., Kochanek, C.S., Udalski, A., et al. 2010, *ApJ*, 708, 927
- Kozłowski, S., Onken, C.A., Kochanek, C.S., et al. 2013a, *ApJ*, 775:92
- Kozłowski, S., Udalski, A., Wyrzykowski, L., et al. 2013b, *AcA*, 63, 1
- Latif, M.A., Schleicher, D.R.G., Schmidt, W., & Niemeyer, J. 2013, *MNRAS*, 433, 1607
- Latif, M.A., & Volonteri, M. 2015, *MNRAS*, 452, 1026
- Li, Y.-R., Wang, J.-M., Ho, L.C., Du, P., & Bai, J.-M. 2013, *ApJ*, 779:110
- LSST Science Collaboration 2009, [arXiv:0912.0201](http://arxiv.org/abs/0912.0201)
- MacLeod, C.L., Ivezić, Ž., Kochanek, C.S., et al. 2010, *ApJ*, 721, 1014
- Merloni, A., Bongiorno, A., Bolzonella, M., et al. 2010, *ApJ*, 708, 137
- Mortlock, D.J., Warren, S.J., Venemans, B.P. et al. 2011, *Nature*, 474, 616
- Murray, N., Quataert, E., & Thompson, T.A. 2005, *ApJ*, 618, 569
- Mushotzky, R.F., Edelson, R., Baumgartner, W., & Gandhi, P. 2011, *ApJ*, 743, L12
- Nelson, C.H., Green, R.F., Bower, G., Gebhardt, K., & Weistrop, D. 2004, *ApJ*, 615, 652
- Onken, C.A., Ferrarese, L., Merritt, D., et al. 2004, *ApJ*, 615, 645
- Pancoast, A., Brewer, B.J., & Treu, T. 2011, *ApJ*, 730, 139
- Pancoast, A., Brewer, B.J., Treu, T., et al. 2014, *MNRAS*, 445, 3073
- Park, D., Kelly, B.C., Woo, J.-H., & Treu, T. 2012, *ApJS*, 203, 6
- Peng, C.Y., Impey, C.D., Ho, L.C., Barton, E.J., & Rix, H.-W. 2006, *ApJ*, 640, 114
- Peterson, B.M. 1993, *PASP*, 105, 247
- Peterson, B.M. 2014, *Space Sci. Rev.*, 183, 253
- Peterson, B.M., Denney, K.D., De Rosa, G., et al. 2013, *ApJ*, 779:109
- Peterson, B.M., Ferrarese, L., Gilbert, K.M., et al. 2004, *ApJ*, 613, 682
- Pozo Nuñez, F., Ramolla, M., Westhues, C., et al. 2012, *A&A*, 545, 84
- Pozo Nuñez, F., Westhues, C., Ramolla, M., et al. 2013, *A&A*, 552, AA1
- Rasmussen, C.E., & Williams, C. K.I. 2006, *Gaussian Processes for Machine Learning* (University Press Group Limited)
- Rybicki, G.B., & Press, W.H. 1992, *ApJ*, 398, 169
- Sergeev, S.G., Doroshenko, V.T., Golubinskiy, Y.V., Merkulova, N.I., & Sergeeva, E.A. 2005, *ApJ*, 622, 129
- Shankar, F. 2009, *New Astron. Rev.*, 53, 57
- Shankar, F., Bernardi, M., & Haiman, Z. 2009, *ApJ*, 694, 867
- Shapovalova, A.I., Popović, L.Č., Burenkov, A.N., et al. 2013, *A&A*, 559:A10
- Shappee, B.J., Prieto, J.L., Grupe, D., et al. 2014, *ApJ*, 788:48
- Sharp, R., Saunders, W., Smith, G., et al. 2006, *SPIE*, 6269, 90G

- Shen, Y. 2013, *BASI*, 41, 61
- Shen, Y., Brandt, W.N., Dawson, K.S., et al. 2015, *ApJS*, 216:4
- Silk, J., & Rees, M.J. 1998, *A&A*, 331, L1
- Soszyński, I., Udalski, A., Poleski, R., et al. 2012, *AcA*, 62, 219
- Tewes, M., Courbin, F., Meylan, G., et al. 2013, *A&A*, 556, A22
- Treu, T., Malkan, M.A., & Blandford, R.D. 2004, *ApJ*, 615, L97
- Udalski, A., Szymanski, M.K., Soszynski, I., & Poleski, R. 2008, *AcA*, 58, 69
- Vanden Berk, D.E., Richards, G.T., Bauer, A., et al. 2001, *AJ*, 122, 549
- Volonteri, M. 2010, *A&AR*, 18, 279
- Wandel, A., Peterson, B.M., & Malkan, M.A. 1999, *ApJ*, 536, 579
- Woo, J.-H., Treu, T., Barth, A.J., et al. 2010, *ApJ*, 716, 269
- Zhang, X.-G. 2013, *MNRAS*, 434, 2664
- Zu, Y., Kochanek, C.S., Kozłowski, S., & Udalski, A. 2013, *ApJ*, 765, 106
- Zu, Y., Kochanek, C.S., & Peterson, B.M. 2011, *ApJ*, 735, 80